J. Fluid Mech. (1993), *vol.* 254, *pp.* 701–719

Turbulence-driven secondary flows and formation of sand ridges

By MARCO COLOMBINI

Istituto di Idraulica, Universitá di Genova,
Via Montallegro 1, 16145 Genova, Italy

(Received 6 May 1992 and in revised form 22 March 1993)

The mechanism of generation of sand ridges, longitudinal stripes observed both in natural rivers and in the laboratory, is investigated with the aim of showing that the initiation mechanism is intrinsically associated with an instability of the erodible bottom rather than with the effect of the secondary vortices induced by the sidewalls as suggested by previous works. A linear stability analysis of flow in infinitely wide channels with an erodible bed is then presented. In order to model the generation of turbulence-driven cellular secondary motions a nonlinear turbulence closure scheme is used. Comparison with published experimental data for the case of air duct flow over a fixed 'ridge-shaped' bed is performed in order to check the performance of the turbulence model and proves satisfactory. It turns out that under suitable conditions the uniform unidirectional flow is unstable with respect to spanwise disturbances with a characteristic wavelength of the order of the flow depth. This theoretical finding is supported by experimental observations on wide open-channel flows. The secondary vortices are directed in such a way as to amplify bed perturbations, eventually leading to the formation of sand ridges irrespective of the presence of the sidewalls.

1. Introduction

Many field observations in straight wide rivers suggest the existence of cellular secondary currents. Periodic spanwise variation of free-surface velocity (Kinoshita 1967) and sediment concentration (Vanoni 1946), often connected with the appearance, on the river bed, of a sequence of longitudinal ridges called 'sand ribbons' or 'sand ridges' (Culberston 1967) have been detected and they invariably exhibit flow depth as a characteristic spatial scale.

Secondary motions in the plane perpendicular to the main streamwise direction of a flow were classified into two categories by Prandtl (see Bradshaw 1987). Secondary flows of the first kind are driven by the curvature effect and exist in both laminar and turbulent flows, while those of the second kind arise only in turbulent flows in straight channels and non-circular ducts with turbulence as a driving mechanism.

Since the pioneering work of Brundett & Baines (1964), several authors (see Gerard 1978 for an extensive review) have studied the mechanics of secondary flow in non-circular conduits, showing that turbulence-driven secondary flows are induced by the imbalance of the normal Reynolds stresses in the cross-sectional plane. Speziale (1982) has introduced a sufficient condition for the development of longitudinal vortices stating that the longitudinal velocity field must give rise to a difference in the normal stresses for the secondary flow to appear.

It may be easily shown that this condition cannot be satisfied if a turbulence closure

model based on the eddy viscosity concept is used. Therefore the standard k–ϵ (or k–l) model is unable to predict the appearance of this kind of cellular secondary motion. A turbulence model able to link the Reynolds stresses with the gradients of the longitudinal velocity field must indeed be used. This applies to, among others, the algebraic stress model (Launder & Ying 1972; Naot & Rodi 1982) and to the nonlinear k–l model of Speziale (1987) that were, in fact, successfully applied to the study of corner secondary flows in square ducts.

Being able to correctly model the production mechanism of secondary motions leaves however unresolved the question of why these vortices should form across the whole width of a sufficiently wide channel. The intensity of the vortices induced by the sidewall decreases rapidly when moving away from the lateral banks. The experimental work of Nezu, Nakagawa & Tominaga (1985) investigated the behaviour of secondary flows in smooth air ducts with different aspect ratios and showed no longitudinal vortices in the central region when the aspect ratio is greater than 5. This behaviour was confirmed by Naot & Rodi (1982) who solved numerically the flow in an open smooth channel.

A possible mechanism of production of stable cellular secondary motions involves both the corner-induced vortices and an erodible bed. Nezu & Nakagawa (1984) postulated that the mild peak in the lateral bed shear stress caused by the presence of the corner secondary flow produces a spanwise variation of the bed-load transport that leads to the formation of a sand ridge. A new vortex will then be created by the presence of this ridge inducing a new peak in the tangential bed shear stress. If this process is recursively repeated, it will eventually cover the whole cross-section. This mechanism has been recently tested experimentally by the same authors (Nezu & Nakagawa 1989) who however noticed that regular patterns of ridges and troughs occurred in the central region even when the sidewall ridge had not yet sufficiently formed. Furthermore, they observed that sand ribbons appeared comparatively quickly over the whole cross-section after the formation of the first one.

The above observations strongly suggest that the basic mechanism underlying the formation of cellular secondary vortices and sand ridges is an instability process as Ikeda (1981) first argued. The presence of the sidewalls would no longer be a necessary ingredient for secondary motions to arise, even though the corner vortex can still act as a further source of disturbances for the central region, an idea that was mentioned briefly also in the work of Nezu & Nakagawa (1989).

The presence of a non-uniform roughness of the bed has often been related to the formation of sand ridges (see, for instance, Tsujimoto 1989). It has already been experimentally demonstrated (Hinze 1973; Müller & Studerus 1979; McLean 1981; Tominaga & Nezu 1991) that a lateral distribution of roughness generates secondary currents over a fixed flat bed.

One may indeed wonder whether such an effect controls the formation of sand ridges (as pointed out by one of the referees). On the other hand observations suggest that ridges form in the laboratory over uniform sediments (Ikeda 1981; Nezu & Nakagawa 1989). Hence, it appears reasonable to first ascertain what is the mechanism which generates ridges in the uniform case and then investigate the (damping or enhancing) role that sediment non-uniformity might play.

In the present paper the turbulence model of Speziale (1987) is used to perform a linear stability analysis of turbulent flow in an infinitely wide channel. The case of flow in an infinitely wide duct with sinusoidal walls is first analysed and a comparison with the experimental work of Nezu & Nakagawa (1984) is performed to finely tune the turbulence model.

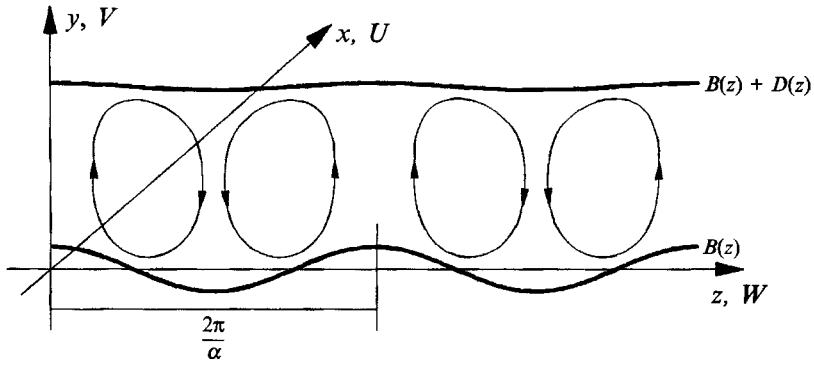

FIGURE 1. Sketch of flow configuration.

The continuity equation for a uniform sediment is then added to the flow equations to solve the complete bed–fluid system. A dispersion relationship that gives the growth rate of a bed perturbation as a function of its wavenumber and of flow and sediment parameters is determined.

The appearance of sand ridges is shown to be controlled by a delicate balance between the stabilizing effect of gravity, that tends to move grains away from the ridges and towards the troughs, and the destabilizing effect of tangential bed shear stress, acting in the opposite direction. Due to the weakness of the secondary vortices (whose intensity is always limited to less than 5 % of the maximum longitudinal velocity), these two terms are of the same order of magnitude for a wide range of variation of flow and sediment parameters. An accurate modelling of the Reynolds stresses is therefore crucial for the formulation of an existence criterion. It will appear that the use of the nonlinear closure scheme of Speziale (1987) is quantitatively not wholly satisfactory but still allows us to show the existence of the instability mechanism.

In the following section the problem of secondary motion in infinitely wide channels is formulated and the choice of the turbulence model is considered. Section 3 is devoted to the linearization process. In §4 the solution for flow in an infinitely wide duct with sinusoidal walls is presented and compared with the experiments. The linear stability analysis of flow over an erodible bottom is presented next and its results are discussed. The final section is devoted to some conclusions and to a discussion on possible future developments.

2. Formulation of the problem

Let us consider flow in a straight, infinitely wide open channel with an erodible bottom as sketched in figure 1. We are concerned here with the explanation of the mechanism of formation of sand ridges, i.e. perturbations of uniform flow which do not exhibit any dependence on the longitudinal coordinate. Hence we will drop all the x-derivative terms in the governing equations.

Neglecting viscous effects, the flow equations can be written in the following dimensionless form

$$\frac{\partial U}{\partial t} + V\frac{\partial U}{\partial y} + W\frac{\partial U}{\partial z} = \frac{S}{Fr^2} + \frac{\partial \tau_{xy}}{\partial y} + \frac{\partial \tau_{xz}}{\partial z}, \tag{2.1}$$

$$\frac{\partial V}{\partial t} + V\frac{\partial V}{\partial y} + W\frac{\partial V}{\partial z} = -\frac{\partial P}{\partial y} + \frac{\partial \tau_{yy}}{\partial y} + \frac{\partial \tau_{yz}}{\partial z}, \tag{2.2}$$

$$\frac{\partial W}{\partial t} + V\frac{\partial W}{\partial y} + W\frac{\partial W}{\partial z} = -\frac{\partial P}{\partial z} + \frac{\partial \tau_{yz}}{\partial y} + \frac{\partial \tau_{zz}}{\partial z}, \tag{2.3}$$

$$\frac{\partial V}{\partial y} + \frac{\partial W}{\partial z} = 0, \tag{2.4}$$

where (U, V, W) are the mean velocity components in the (x, y, z) directions respectively, t is time, τ_{ij} are the Reynolds stresses, S is the longitudinal slope, Fr is the unperturbed Froude number, and P is the difference between the total pressure and the hydrostatic pressure $(1 - y)/Fr^2$.

Variables have been made non-dimensional in the form

$$(U^*, V^*, W^*) = U_0^*(U, V, W), \qquad (P^*, \tau_{ij}^*) = \rho U_0^{*2}(P, \tau_{ij}),$$

$$(x^*, y^*, z^*) = D_0^*(x, y, z), \qquad (B^*, D^*) = D_0^*(B, D),$$

$$t^* = \frac{D_0^*}{U_0^*}t,$$

where U_0^*, D_0^* denote average speed and depth for the uniform unperturbed flow, ρ is fluid density while D^* and B^* are the local depth and the bottom shape respectively.

The continuity equation for sediment, assuming bed-load only, reads

$$\frac{\partial B}{\partial t} = -\hat{Q}\frac{\partial Q}{\partial z}, \tag{2.5}$$

where Q is the dimensionless sediment flow rate in the spanwise direction and

$$\hat{Q} = \frac{d_s^*[(s-1)gd_s^*]^{\frac{1}{2}}}{(1-p_s)D_0^*U_0^*}$$

is the ratio between the commonly used scale of sediment discharge and the flow rate. In the above equation d_s^*, s and p_s are respectively grain size, relative density and porosity of the sediment, assumed uniform, while g is the gravitational acceleration.

Modelling the influence of gravity on the direction of bed-load motion as suggested by Ikeda (1982) (see also Parker 1984) we finally write

$$Q = \Phi(\theta)\left(\frac{\tau_t}{\tau} - \frac{r}{\theta^{\frac{1}{2}}}\frac{\partial B}{\partial z}\right), \qquad \Phi(\theta) = 8(\theta - 0.047)^{\frac{3}{2}}, \tag{2.6a,b}$$

where θ is the Shields parameter, r is a constant assumed as 0.3, τ is the amplitude of the bottom shear stress, τ_t is the component of the bed shear stress in the direction tangential to the bed itself, and $\Phi(\theta)$ is the Meyer Peter–Müller load function.

An analysis of the characteristic timescales of flow and bed evolution shows that the latter is much slower, due to the smallness of the parameter $\hat{Q}$, which typically ranges from 10^{-3} to 10^{-5}. If a new time variable $T = \hat{Q}t$ is formally introduced, derivatives with respect to T can be neglected in the momentum equations so that the problem can be solved as a quasi-steady flow over a slowly varying erodible bottom. Following this approach no coupling exists between flow equations and the sediment continuity equation because the flow field is supposed to instantaneously adapt to bed variations.

As mentioned earlier the turbulence closure model must be able to relate the Reynolds stresses to the gradients of the longitudinal flow velocity in order to reproduce turbulence-driven secondary flows. A glance at the equation for the mean streamwise vorticity ω

$$\frac{\partial \omega}{\partial t} + V\frac{\partial \omega}{\partial y} + W\frac{\partial \omega}{\partial z} = \frac{\partial^2}{\partial y \partial z}(\tau_{zz} - \tau_{yy}) + \left(\frac{\partial^2}{\partial y^2} - \frac{\partial^2}{\partial z^2}\right)\tau_{yz} \tag{2.7}$$

reveals that the right-hand side of the equation acts as a source term for the vorticity. It is quite clear that if this term does not depend on the longitudinal velocity field, the equation is uncoupled from the streamwise momentum equation and the unidirectional flow solution is the only solution of the problem.

In Speziale's model a constitutive relationship is derived as a higher-order approximation of the usual linear relationship for the Reynolds stress tensor

$$\tau_{ij}^L = -\tfrac{2}{3}k\delta_{ij} + 2\nu_t D_{ij}, \tag{2.8}$$

where k is the turbulent kinetic energy, D_{ij} is the mean rate of strain tensor, $\nu_t = \frac{1}{2}k^{\frac{1}{2}}l$ is the eddy viscosity and l is the turbulence lengthscale.

The next higher approximation of the above equation is obtained by Speziale on a purely deductive basis after assuming τ to be a function of the form

$$\tau = \tau\left[\nabla\vec{v}, \frac{\mathrm{D}(\nabla\vec{v})}{\mathrm{D}t}, k, l\right]. \tag{2.9}$$

Imposing that some general properties of the Navier–Stokes equation (coordinate and dimensional invariance, positiveness of k and material frame-indifference) be satisfied, Speziale derives at second order the following constitutive relationship:

$$\tau_{ij} = \tau_{ij}^L + C_D l^2(D_{im}D_{mj} - \tfrac{1}{3}D_{mn}D_{mn}\delta_{ij}) + C_E l^2(\widehat{D_{ij}} - \tfrac{1}{3}\widehat{D_{mm}}\delta_{ij}), \tag{2.10}$$

where

$$\widehat{D_{ij}} = \frac{\mathrm{D}D_{ij}}{\mathrm{D}t} - \frac{\partial U_i}{\partial x_k}D_{kj} - \frac{\partial U_j}{\partial x_k}D_{ki}.$$

Following this approach, only two new constants (C_D and C_E) are introduced, which will be determined by comparison with experimental data.

Once the Boussinesq hypothesis of linearity has been removed, thus creating the necessary link between the longitudinal flow field and the secondary flow, the structure of ν_t and l is taken here to be adequately represented by perturbing simple algebraic relationships known to hold for a uniform flow. This approach is likely to be inaccurate when turbulence dynamics has a strong influence on the flow field but might be appropriate in this context, where secondary flows appear as a consequence of (small) geometric variations of bed topography. With that in mind, the nonlinear k–l model of Speziale (1987) was the natural choice.

On the other hand, algebraic stress models like the one proposed by Naot & Rodi (1982) or the more complete one proposed by Demuren & Rodi (1984) are implicit in nature and are not derived by general principles on the basis of simple assumptions. Nevertheless, we want to stress here that, once the linearization process has been completed, the dependence of Reynolds stresses on the mean strain rate has close similarity to that of the Naot & Rodi algebraic stress model, which was successfully used to predict secondary flow in non-circular ducts.

The structure of ν_t and l could more appropriately be obtained as a solution of the full nonlinear k–l model by which both the turbulent energy k and the lengthscale l are 'transported' through suitable transport equations. However, the approach chosen herein strongly simplifies the computational work. The absence of separation phenomena due to the peculiar structure of sand ridges was also encouraging in the assumption of local equilibrium implied by this choice.

3. Linearization

In this section the conditions under which the two-dimensional uniform flow loses stability to perturbations periodic in the spanwise direction are studied. The amplitude of such disturbances is supposed to be small enough for linearization to be a valid approach. Disturbed flows of the kind

$$\begin{aligned}(U, V, P) &= (U_0(y), 0, P_0(y)) + \epsilon \exp(\sigma T)(u(y), v(y), p(y)) \cos(\alpha z),\\ W &= -\epsilon \exp(\sigma T)\alpha w(y) \sin(\alpha z),\\ (B, D) &= (0, 1) + \epsilon \exp(\sigma T)(1, d) \cos(\alpha z),\\ Q &= -\epsilon \exp(\sigma T)\alpha q \sin(\alpha z),\\ (\nu_t, l) &= (\nu_{t0}(y), l_0(y)) + \epsilon \exp(\sigma T)(\nu(y), \lambda(y)) \cos(\alpha z),\end{aligned}$$

will be investigated with ϵ being a small (strictly infinitesimal) parameter that plays the role of the amplitude of the bed perturbation with growth rate σ and wavenumber α.

The non-orthogonal coordinate transformation

$$\eta = \frac{y - B(z)}{D(z)}, \qquad \zeta = z,$$

which maps the cross-section on a rectangular domain, has been adopted.

Making the necessary substitutions and collecting terms of order ϵ^0, the system of differential equations for the basic uniform flow reads

$$\nu'_{t0} U'_0 + \nu_{t0} U''_0 = -C_0, \tag{3.1}$$

$$P'_0 - (\tfrac{1}{6} C_D + \tfrac{2}{3} C_E)(l_0 l'_0 U'^2_0 + l_0^2 U'_0 U''_0) = 0, \tag{3.2}$$

where primes denote derivatives with respect to η while

$$C_0 = \frac{u_{*0}^2}{U_0^{*2}} = \frac{S}{Fr^2}$$

is a friction coefficient and u_{*0} is the friction velocity for the uniform unperturbed flow.

At first order in ϵ, after some manipulations and a considerable amount of algebra, a system of ordinary differential equations is eventually obtained that can be written in the general form

$$\mathbf{D}\boldsymbol{Z} = d\,\boldsymbol{T} + \boldsymbol{R}, \tag{3.3}$$

where d is considered as a parameter to be determined and

$$\boldsymbol{Z} = \begin{pmatrix} u \\ v \\ w \\ p \end{pmatrix}.$$

The linear differential operator **D** is reported in Appendix A, as are the two vectors $\boldsymbol{T}, \boldsymbol{R}$ that depend only on basic flow quantities.

The above system has to be solved with appropriate sets of boundary conditions, which will be made explicit in the next sections for the two cases examined. The solution has been obtained numerically using a shooting method with a Runge–Kutta integration scheme.

More precisely, linearity of the differential system allows us to express its solution in the form

$$\boldsymbol{Z} = \sum_{i=1}^{3} c_i \boldsymbol{Z}_i + d\boldsymbol{Z}_{\mathrm{T}} + \boldsymbol{Z}_{\mathrm{R}}. \tag{3.4}$$

Thus $\boldsymbol{Z}$ is a linear combination of three linearly independent solutions of the homogeneous initial value problem

$$\mathbf{D}\boldsymbol{Z} = 0$$

each satisfying the boundary conditions at the lower boundary, plus particular solutions of the non-homogeneous differential systems

$$\mathbf{D}\boldsymbol{Z} = \boldsymbol{T}, \qquad \mathbf{D}\boldsymbol{Z} = \boldsymbol{R}$$

still satisfying the lower boundary conditions.

The constants c_1, c_2, c_3 and d are then determined by solving the linear algebraic non-homogeneous system obtained by imposing the remaining conditions at the upper boundary.

As far as the sediment continuity equation is concerned, linearization yields the following equation for the growth rate of bed perturbations:

$$\frac{\sigma}{\Phi(\theta_0)\alpha^2} = \left[\frac{w'}{U_0'}\right]_{\eta_0} - \frac{r}{\theta_0^{\frac{1}{2}}}, \tag{3.5}$$

where θ_0 is the Shields parameter for the basic uniform flow, and a positive w' at the bottom corresponds to a secondary flow moving from the trough towards the ridge. The above equation clearly shows that the sign of the growth rate (and then the amplification or decay of bed perturbations) is the result of a balance between the two counteracting effects of tangential bed shear stress and gravity.

In the following sections the solution procedure presented above will be employed for the cases of confined flow over a fixed sinusoidal bottom and open-channel flow over an erodible bed.

4. Confined flow over a fixed sinusoidal bottom

The need to ascertain the intensity of secondary flows induced by the presence of ridges was appreciated by Nezu & Nakagawa (1984) who studied air flow in a smooth rectangular duct in which longitudinal stripes of trapezoidal section were attached onto both the lower and the upper wall to simulate sand ribbons.

They performed detailed hot-wire anemometric measurements of the three components of the velocity vector and provided contour plots showing the behaviour of the Reynolds stresses in the cross-sectional plane.

This section is devoted to a comparison between the results obtained through the present theory and the experimental data (Nezu & Nakagawa 1984) in order to check the consistency of the turbulence model adopted herein and identify the most appropriate values of the constants C_D and C_E.

In his paper Speziale determined such constants by making use of just one experimental point for the normal stress differences. We will focus our attention on the behaviour and on the intensity of the difference of the normal stresses in the cross-sectional plane, the 'production' term for the secondary flow, as a function of these constants.

The symmetry of the problem now implies $D = 1 - B$ and consequently $d = -1$ in the differential system (3.3). The fact that the value of d is fixed is consistent with the diminished number of boundary conditions.

The no-slip condition is imposed at $y = B + \eta_0(1 - B)$, namely at a distance $\eta = \eta_0$ from the bed, where η_0 is the non-dimensional conventional reference level for no slip under uniform conditions. At the plane of symmetry $\eta = 1$, symmetry conditions are imposed that read

$$u' = w' = v = 0. \tag{4.1}$$

Furthermore we follow Gerard (1978) and set

$$l = f(\eta)D, \qquad \nu_t = f(\eta)\frac{u_*}{U_0^*}D, \tag{4.2a,b}$$

where

$$f(\eta) = a\eta(2 - \eta)[(1 - \eta)^2 + b],$$

$$a = \frac{\kappa - 0.14}{2}, \qquad b = \frac{0.14}{\kappa - 0.14},$$

and κ is the von Kármán constant taken as 0.4. Alternative forms of the function f have been tried (Nikuradse (see Schlichting 1979); Travis, Buhr & Sesonske 1971) producing similar results. This choice yields the following structure for l and ν_t at various orders in ϵ:

$$l_0 = f(\eta), \qquad \nu_{t0} = C_0^{\frac{1}{2}} f(\eta); \tag{4.3a,b}$$

$$\lambda = l_0 d, \qquad \nu = \nu_{t0}\left(d + \left[\frac{u'}{U_0'}\right]_{\eta_0}\right). \tag{4.4a,b}$$

Finally the quantities C_0 and η_0 have been determined assuming the usual log-law distribution for smooth walls by which

$$C_0^{-\frac{1}{2}} = 3 + 2.5\ln(Re\, C_0^{\frac{1}{2}}),$$

$$\eta_0 = \exp(-\kappa C_0^{-\frac{1}{2}} - 1),$$

where Re is the Reynolds number, set to a value of 13 000 as in the experiments of Nezu & Nakagawa.

As outlined in the previous section, when symmetry conditions (4.1) are imposed using the splitting (3.4), a 3×3 linear algebraic system is obtained, the solution of which gives the values of the three unknowns c_i.

In order to simulate the sharp changes in the bottom topography due to the presence of the trapezoidal ridges used by Nezu & Nakagawa, the bed was Fourier-analysed and the solutions corresponding to various harmonics were superimposed. Four harmonics were used for the wider case ($L = 2D_0^*$, with L the spacing between two consecutive ridges) and two for the narrower ($L = D_0^*$).

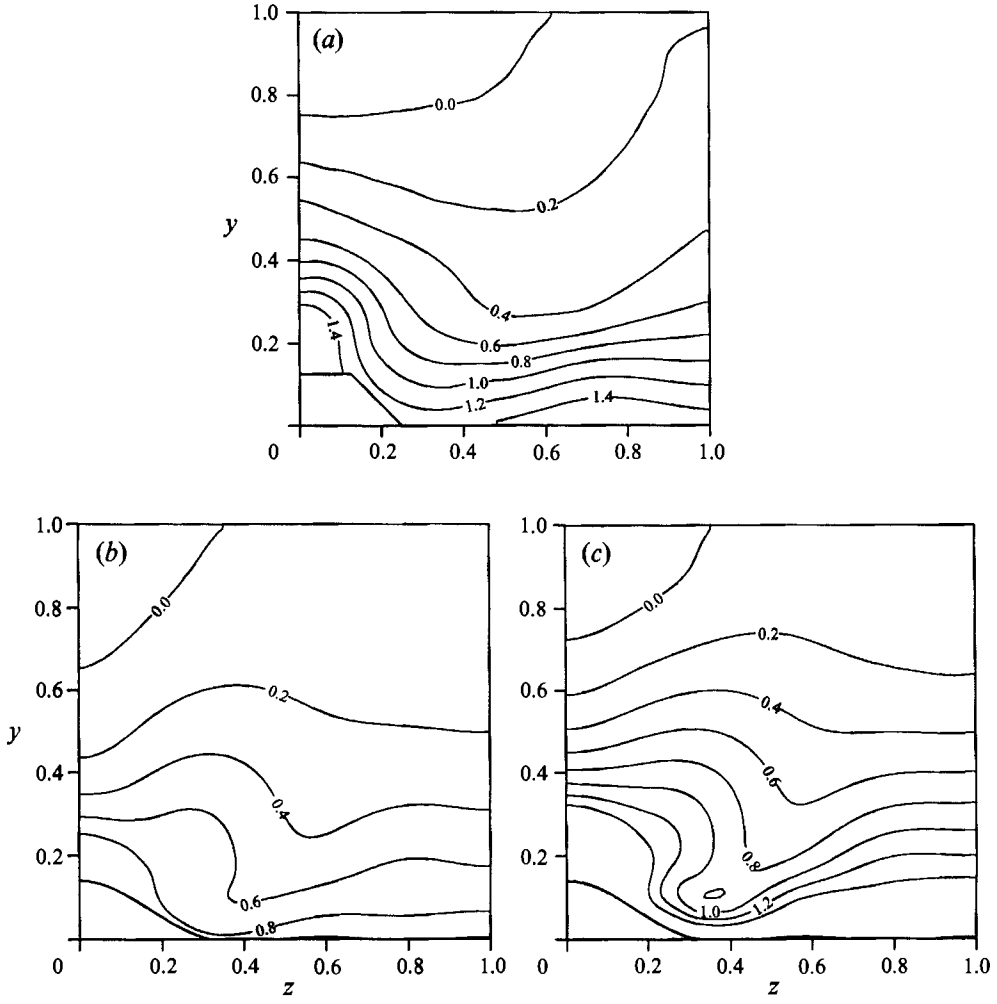

FIGURE 2. Contour lines of $(\tau_{zz} - \tau_{yy}) \times 10^3$. (*a*) Experiments of Nezu & Nakagawa (1984) (NN); (*b*) present theory, $C_D = C_E = 1.68$; (*c*) present theory, $C_D = C_E = 3.4$.

Speziale (1987) proposed a value of 1.68 for both the constants C_D and C_E. This value, which was tested first, produced a secondary flow weaker than the experimental one. The maximum velocity in the cross-sectional plane was found to attain a value of about 0.8% of the maximum streamwise velocity U_{max}, less than half the value found in the experiments. Also the overall difference in the normal stresses was smaller than the observed one as shown in figures 2 (*a*) and 2 (*b*).

Several combinations of the values of the two constants were tested in order to achieve a better performance of the model. Assuming $C_D = C_E = C$ and increasing C leads to an intensification of the secondary vortex until a value of C equal to 3.4 is reached. A further increase of C does not lead to a corresponding increase in the intensity of the secondary flow. Numerical experiments were also performed in order to assess the sensitivity of the model to the variation of each constant. However, the use of different values for C_D and C_E always led to a poorer prediction in terms of the amplitude of the difference of normal stresses, or of the vorticity intensity and

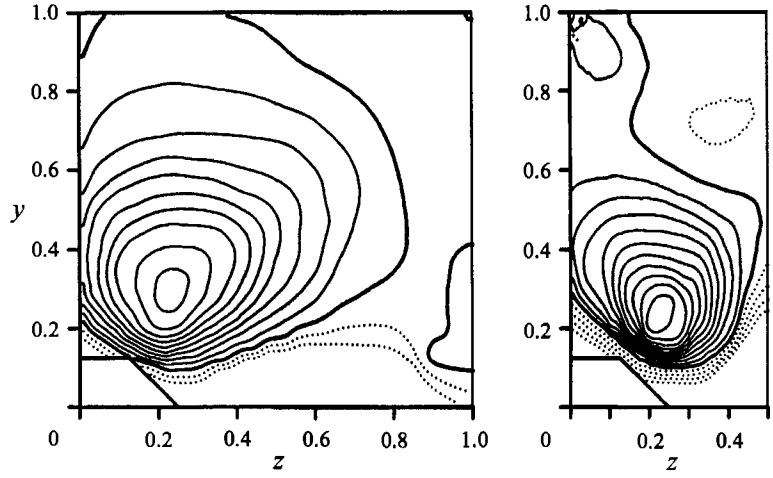

FIGURE 3. Contour lines of vorticity ω. Experiments (NN). Contour increment is 0.02. Dotted lines correspond to negative values, solid lines correspond to positive values; the thick solid line corresponds to a value of zero.

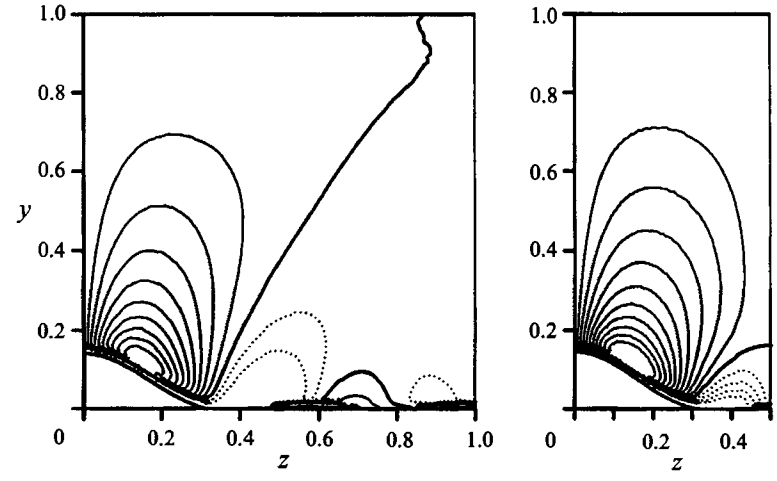

FIGURE 4. Contour lines of vorticity ω. Present theory, $C_D = C_E = 3.4$. Contour increment is 0.02; for legend see figure 3.

distribution or of the velocity intensity and distribution. Hence, the value of 3.4 was adopted as the optimum choice for both constants.

With this choice the difference of normal stresses $\tau_{yy} - \tau_{zz}$ is shown in figure 2(c) and it satisfactorily compares with the corresponding contour plot presented by Nezu & Nakagawa, both in the spatial behaviour and in the value of the maximum occurring over the ridge. The maximum streamwise velocity now attains a value of $0.015U_{max}$.

We want to point out that, at least for the range of values tested, the process of varying the constants affects mostly the intensity of the secondary flow but has only a minor influence on the pattern of the secondary flow itself, thus suggesting that the balance between the various terms proportional to C_D and C_E in the equation is not dramatically altered by the process of tuning.

In figures 3, 4, 5 and 6 the comparison is extended to the vorticity and to the

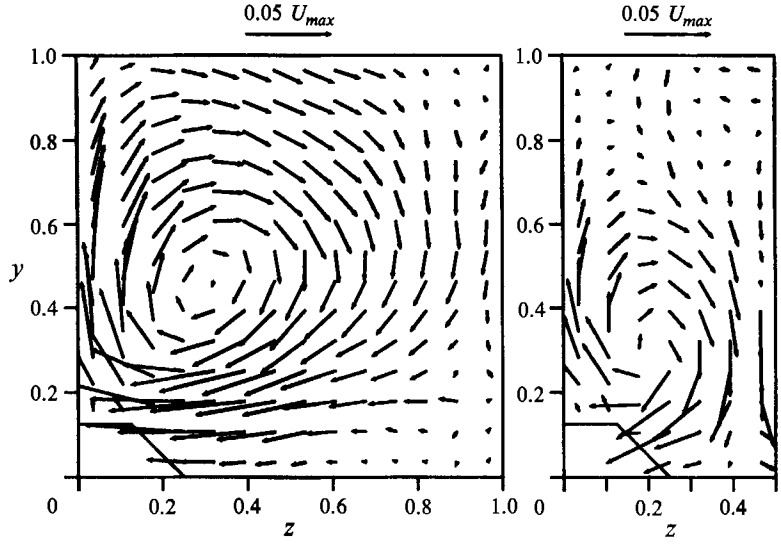

FIGURE 5. Flow pattern of secondary currents. Experiments (NN).

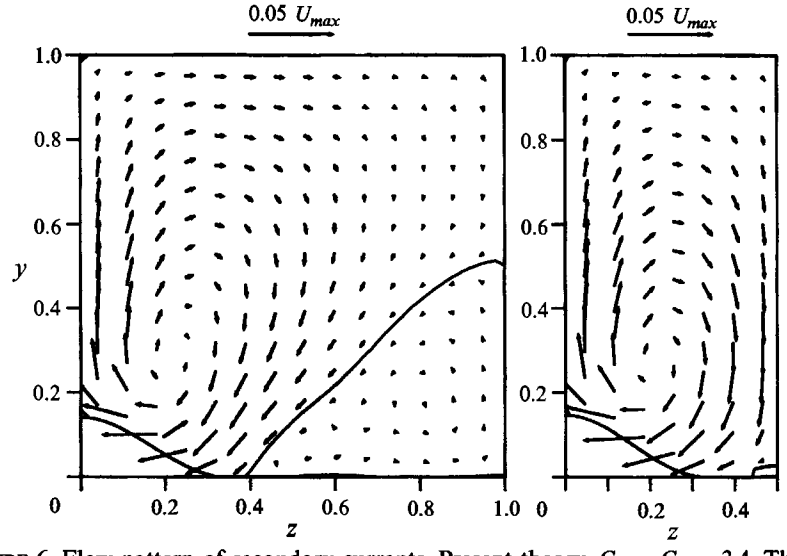

FIGURE 6. Flow pattern of secondary currents. Present theory, $C_D = C_E = 3.4$. The solid line separates areas of counter-rotating fluid.

secondary flow field for the two cases analysed in the experiments. The effect of higher harmonics of the bed profile is evident in the wider case in which a weaker 'secondary' vortex can be easily identified in the theoretical solution. Although barely noticeable in the experimental vector plots, its existence is strongly suggested both by the presence of a negative vorticity area close to the trough and by the observed behaviour of the main vortex. Experiments show in fact that the main vortex is pushed towards the ridge, its centre lying at a distance equal to $L/8$ from the ridge. In the narrower case, in which the slope of the bottom is closer to a cosine curve, the configuration is more symmetric and the centre of the cellular vortex is set at

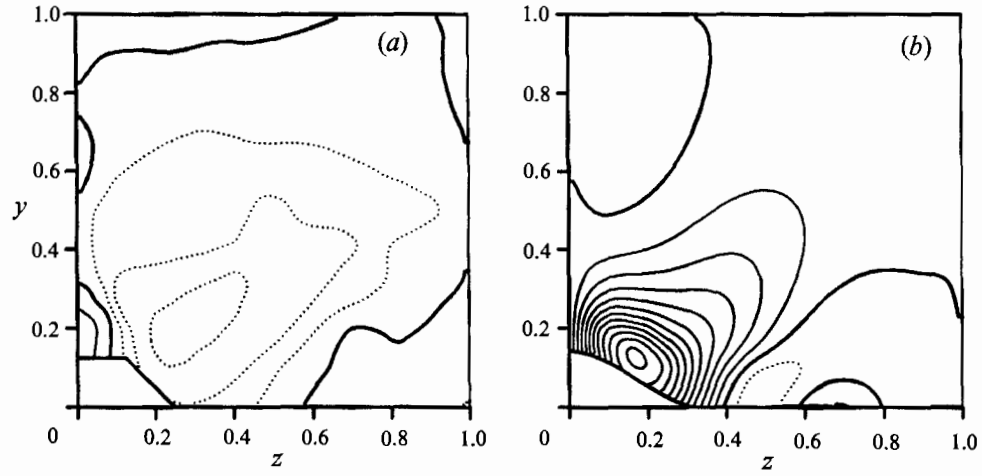

FIGURE 7. Contour lines of $\tau_{yz} \times 10^3$. (*a*) Experiments (NN); (*b*) present theory, $C_D = C_E = 3.4$. Contour increment is 0.01; for legend see figure 3.

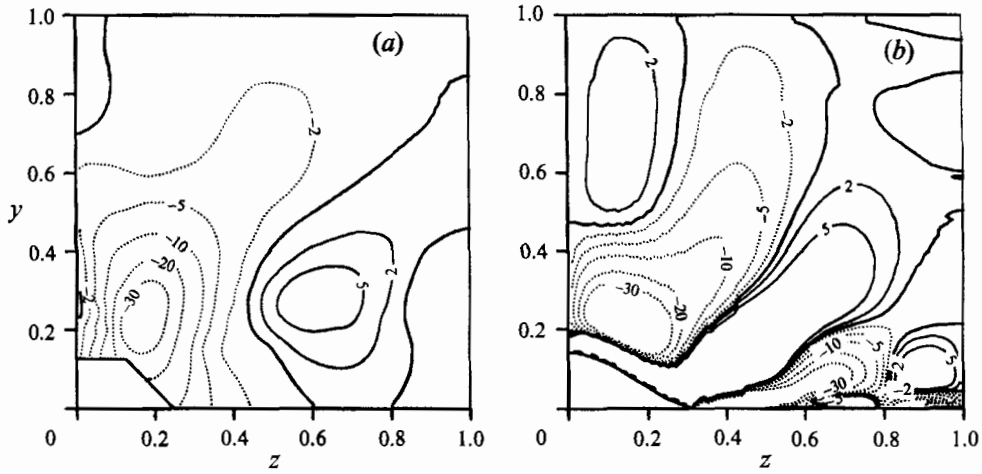

FIGURE 8. Contour lines of 'production' term $(\partial^2/\partial y \partial z)/(\tau_{zz} - \tau_{yy}) \times 10^3$. (*a*) Experiments (NN); (*b*) present theory, $C_D = C_E = 3.4$. For legend see figure 3.

$L/4$ from the ridge. The presence of this secondary vortex is also responsible for the upflow over the ridge being noticeably stronger than the downflow, a feature recognized both in the experiments and in field observation of actual rivers (Jackson 1976).

The comparison with the experiments, even in the context of a linear framework like the one adopted herein, seems satisfactory, with the only noticeable exception of the transverse Reynolds stress τ_{yz} which shows a poor agreement with the experimental measurements, both quantitatively and qualitatively (figure 7*a*, *b*).

Nezu & Nakagawa were well aware of the fact that the experimental precision of τ_{yz} was lower than that of the other Reynolds stresses because the X-wire procedure adopted for the measurement of this quantity involved the rotation of the probe to three different angles instead of the simultaneous measurements of V and W.

Nevertheless this discrepancy in a quantity that, as it will soon be shown, plays a key role in the dynamics of the bed, deserves further comment.

The vorticity balance (2.7) may be recalled to shed some light on this apparent inconsistency. The convective terms on the left-hand side are of higher order with respect to the two terms appearing on the right-hand side, a fact that is clearly confirmed by the experiments. At order ϵ the vorticity equation reduces then to a balance between the production term, involving the difference of the normal stresses, and the term related to the tangential stress τ_{yz}. Our prediction of the production term is in good agreement with the experimental plots (see figure 8*a*, *b*), namely the qualitative pattern is the same (regions of positive and negative production appear to be correctly predicted) and the quantitative agreement is reasonable.

This result, together with the fact that Nezu & Nakagawa were unable to use the measured values of tangential stress to evaluate this term ' ... because these second-differential values indicated a large scatter ...', seems to indicate that the inability to predict the spanwise tangential stress with the same degree of success might be largely due to experimental inaccuracy.

5. Open-channel flow over an erodible bottom: sand-ridge formation

We now proceed to investigate the time evolution of bed disturbances. It will be shown that, under suitable conditions, spanwise perturbations that experience an amplification in time do exist.

The velocity vector must again vanish at the bed, while at the free surface the dynamic and kinematic conditions read

$$v_{t0}(v + w') + \tfrac{1}{4}C_D l_0^2 U_0' u = 0, \tag{5.1}$$

$$2v_{t0}u' + (\tfrac{1}{2}C_D - \tfrac{3}{2}C_E)l_0^2 U_0'\alpha^2 w + \tfrac{1}{2}C_E l_0^2 U_0'' v = 0, \tag{5.2}$$

$$-p + d/Fr^2 + 2v_{t0}\alpha^2 w + (\tfrac{1}{6}C_D + \tfrac{2}{3}C_E)l_0^2 U_0' u' = 0, \tag{5.3}$$

$$v = 0. \tag{5.4}$$

As in De Vriend (1977) the mixing-length hypothesis

$$\nu_t = l^2 \frac{\partial U}{\partial y}$$

is adopted, where l is chosen such as to produce a logarithmic profile for the basic flow and reads

$$l = g(\eta)D, \tag{5.5}$$

with

$$g(\eta) = \kappa\eta(1-\eta)^{\frac{1}{2}}.$$

At order ϵ^0 and ϵ respectively, this choice leads to

$$l_0 = g(\eta), \qquad v_{t0} = l_0^2 U_0'; \tag{5.6a,b}$$

$$\lambda = l_0 d, \qquad v = v_{t0}\left(d + \frac{u'}{U_0'}\right), \tag{5.7a,b}$$

while the friction coefficient C_0 is now (rough wall)

$$C_0^{-\frac{1}{2}} = 6 - 2.5\ln(2.5d_s).$$

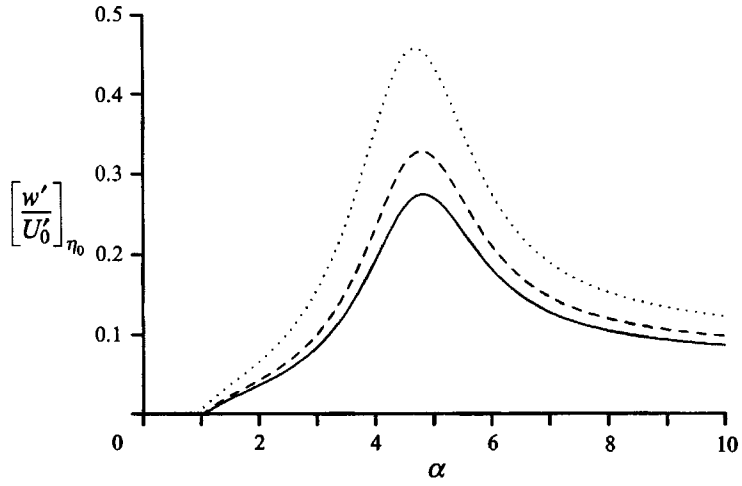

FIGURE 9. Destabilizing term $[w'/U_0']_{\eta_0}$ as a function of the wavenumber α for different values of the relative roughness: ——, $d_s = 0.005$; – – – –, $d_s = 0.01$; · · · · · ·, $d_s = 0.05$.

Imposing the four boundary conditions at the free surface leads to a non-homogeneous algebraic system in the four unknowns c_1, c_2, c_3 and d that gives the response of the fluid to a bed disturbance of amplitude ϵ. Substitution of this solution into (3.5) yields a dispersion relationship among the parameters that can be written in the general form

$$F(\sigma, \alpha, d_s, Fr) = 0. \tag{5.8}$$

For given d_s and Fr, σ depends on the wavenumber α. As shown in (3.5) the sign of σ is determined by a balance between a 'destabilizing' term, related to the bed shear stress component in the direction tangential to the bed, and the stabilizing effect of gravity. In figure 9 the destabilizing term $[w'/U_0']_{\eta_0}$ is plotted versus the wavenumber α, with the relative roughness d_s as a parameter; its behaviour is almost unaffected by changes in the Froude number. The effect of gravity is to shift vertically the entire plot by the amount $-r/\theta_0^{\frac{1}{2}}$. This quantity is inversely proportional to Fr through θ_0, which reads

$$\theta_0 = Fr^2 \frac{C_0}{(s-1)d_s}. \tag{5.9}$$

Thus it is clear that an underestimation of the destabilizing term will eventually lead to an overestimation of the critical Froude number, defined as the Froude number at which the action of gravity exactly balances that of the shear stress.

The role played by the Froude number in the present calculation needs to be clarified.

As far as the flow field solution is concerned, the Froude number has an influence only on the amplitude of free-surface perturbations. These undulations appear as a consequence of bed perturbation and have only a minor effect on the amplitude and structure of secondary flow, which is essentially 'turbulence-driven'. The small Fr dependence of the destabilizing term plotted in figure 9 follows.

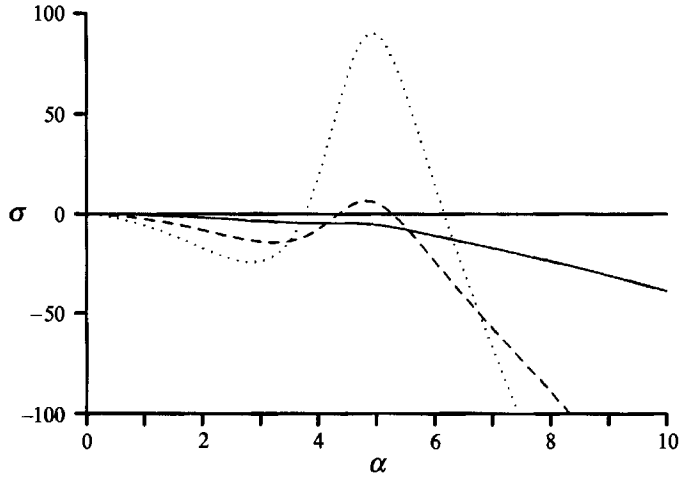

FIGURE 10. Growth rate of bed perturbations σ as a function of the wavenumber α for $d_s = 0.01$ and for different values of the Froude number: ——, $Fr = 1$; – – – –, $Fr = 2$; · · · · · ·, $Fr = 3$.

When an erodible bed is considered, the value of the Shields parameter for the basic uniform flow θ_0 is fixed once d_s and Fr are fixed, as shown by (5.9). A higher Froude number corresponds then to a higher basic sediment transport and its influence on the appearance of sand ridges is much stronger than on the intensity of the secondary flow.

In figure 10 the behaviour of the growth rate σ, for a value of the relative roughness d_s of 0.01, is presented as a function of the wavenumber α with the Froude number as a parameter.

It can be seen that for $Fr = 1$ the unidirectional uniform flow is stable. When the value of the Froude number is raised, unstable disturbances can develop leading to a spanwise periodic three-dimensional flow. Disturbances with a wavenumber of about 4.8 exhibit the maximum growth rate.

The present analysis therefore predicts the existence of a region of instability for spanwise bed perturbations with a characteristic wavelength of the order of the flow depth. As stated before, the 'supercritical' behaviour of sand ridges is almost incidental and probably related to an underestimation of the destabilizing term.

To the author's knowledge, the only experimental data available for comparison are those of Kinoshita and Wolman & Brush as reported by Ikeda (1981), a single experiment of Nishiya & Makino (NM) as reported by Hayashi, Ohashi & Kotani (1985), and those contained in the recent paper by Nezu & Nakagawa (1989) (NN). Although information about the complete set of flow and sediment parameters involved in each run is not sufficient to allow a detailed comparison, a qualitative comparison with existing observations on sand ridges has been attempted.

In the experiments reported by Ikeda (1981) the characteristic wavenumber ranges from 2.5 to 4, almost centred around a value of π which represents a spanwise periodicity that is exactly twice the depth. The value of 4.8 predicted by the present theory describes shorter perturbations, with a wavelength 1.3 times the flow depth, a configuration that matches very well the one obtained in the NM experiment. A comparison between the experimental conditions of the NM and NN experiments suggests the possibility that the wavelength can be strongly influenced by the presence

of the sidewalls if the aspect ratio is not sufficiently high. In fact the data of the two experiments differ essentially in the aspect ratio (25 for NM and 11 for NN) and in the measured value of the wavenumber, 4.8 for NM and 2.6 for NN.

The bed topography of the experiment of NM shows however a fairly regular sequence of almost 20 ridges and troughs, while the velocity field measured by NN over a naturally developed sand ribbon bed shows a complex flow structure, with fewer and wider vortices, the two main vortices closer to the centreline rotating in the same direction, so that it is really difficult to recognize any periodic behaviour and even more difficult to identify a characteristic wavelength.

With regard to the critical Froude number, the experimental work shows that ridges appear for Froude numbers ranging from 0.5 to 2. As discussed above, the overestimation of the critical Froude number for instability is bound to be caused by an underestimation of the tangential bed shear stress. This implies that the destabilizing effect on the sediment bottom is underestimated by the present theory.

In this respect it may be worth mentioning the work of Demuren & Rodi (1984) who, testing the simplifying assumptions usually adopted in the algebraic-stress models, discovered that, in the structure of the tangential Reynolds stress, terms that are cubic in the gradients of the velocity field are not negligible within most of the domain. This fact suggests that a higher-order closure scheme may be necessary for an accurate modelling of the tangential Reynolds stresses.

In spite of the limitations of the present results, we do regard as an important achievement having shown that a bottom instability driven by secondary flows is indeed feasible and independent of the presence of sidewalls.

6. Conclusions

A linear stability analysis of flow in infinitely wide channels with an erodible bottom has been presented, showing that the uniform flow can lose stability to perturbed configurations that are spanwise periodic and still uniform in the longitudinal direction.

This instability mechanism can explain the formation of sand ridges when the basic flow does not depend on the lateral coordinate, i.e. when the aspect ratio is reasonably high, eliminating the need for the corner-induced vortex as the initiation mechanism.

The nonlinear turbulence closure of Speziale that we used is capable of providing a non-zero difference of the normal Reynolds stresses in the cross-sectional plane, a necessary condition for the generation of turbulence-driven secondary flows.

The 'forced' solution of cellular vortices generated by a sinusoidal fixed bottom is used to ascertain the performance of this fairly new closure hypothesis, showing that, with an appropriate choice of the constants of the model, a flow field consistent with the experiments is obtained. When the comparison is extended to the Reynolds stress tensor, some discrepancies are found, especially in the behaviour of the spanwise tangential shear stress. This seems to be at least partly due to experimental inaccuracy. The possibility that an even higher-order turbulence closure should be adopted in order to achieve more accurate modelling of tangential stresses needs to be investigated.

When the stability of the whole fluid–bed system is studied, for each fixed value of d_s a critical Froude number that bounds the unstable region and information on the wavelength of the most unstable disturbances are found. Predictions of the

characteristic wavenumber agree with the experiments if the aspect ratio is sufficiently high, while the threshold value of Fr for instability is overestimated, probably due to an underestimation of the bed shear stress.

Secondary currents may also be generated by a non-uniformity of bed roughness. Since grain sorting is known to accumulate fine sand over the ridges and the secondary flow induced by changes in bed roughness is directed, near the bed, from the rough part towards the smooth one, a stronger destabilizing effect can be obtained if the hypothesis of uniform sediment is removed. A more detailed modelling of turbulence quantities, possibly involving a transport equation for the turbulent kinetic energy k, would probably become necessary if such effect has to be considered.

The author is most grateful to Professor G. Seminara for his advice and discussion on various issues regarding this research. This work has been supported by the Italian Ministero dell'Università e della Ricerca Scientifica e Tecnologica under grants MURST 40% and 60%.

Appendix A

The linear differential operator $\mathbf{D}$ can be written in the form

$$\mathbf{D} = \begin{pmatrix} d_{11} & d_{12} & d_{13} & d_{14} \\ d_{21} & d_{22} & d_{23} & d_{24} \\ d_{31} & d_{32} & d_{33} & d_{34} \\ d_{41} & d_{42} & d_{43} & d_{44} \end{pmatrix},$$

where

$$d_{11} = A(\nu_{t0}\mathrm{d}^2/\mathrm{d}\eta^2 + \nu'_{t0}\mathrm{d}/\mathrm{d}\eta) - \alpha^2\nu_{t0},$$

$$d_{12} = -[U'_0 + (\tfrac{1}{4}C_D - \tfrac{1}{2}C_E)\alpha^2 l_0^2 U'_0 - C_E l_0 l'_0 U''_0 - \tfrac{1}{2}C_E l_0^2 U'''_0],$$

$$d_{13} = (\tfrac{1}{4}C_D - \tfrac{1}{2}C_E)\alpha^2 l_0^2 U'_0 \mathrm{d}/\mathrm{d}\eta + [(\tfrac{1}{2}C_D - \tfrac{3}{2}C_E)\alpha^2(2l_0 l'_0 U'_0 + l_0^2 U''_0) + \tfrac{1}{2}C_E\alpha^2 l_0^2 U''_0],$$

$$d_{14} = 0;$$

$$d_{21} = (\tfrac{1}{6}C_D + \tfrac{2}{3}C_E)[l_0^2 U'_0 \mathrm{d}^2/\mathrm{d}\eta^2 + (2l_0 l'_0 U'_0 + l_0^2 U''_0)\mathrm{d}/\mathrm{d}\eta] - \tfrac{1}{4}C_D\alpha^2 l_0^2 U'_0,$$

$$d_{22} = -\alpha^2\nu_{t0}, \qquad d_{23} = \alpha^2\nu_{t0}\mathrm{d}/\mathrm{d}\eta + 2\alpha^2\nu'_{t0}, \qquad d_{24} = -\mathrm{d}/\mathrm{d}\eta;$$

$$d_{31} = -(\tfrac{1}{12}C_D - \tfrac{2}{3}C_E)l_0^2 U'_0 \mathrm{d}/\mathrm{d}\eta + \tfrac{1}{4}C_D(2l_0 l'_0 U'_0 + l_0^2 U''_0),$$

$$d_{32} = \nu'_{t0}, \qquad d_{33} = d_{11}, \qquad d_{34} = -1;$$

$$d_{41} = 0, \qquad d_{42} = \mathrm{d}/\mathrm{d}\eta, \qquad d_{43} = -\alpha^2, \qquad d_{44} = 0.$$

The value of the constant A is 2 for the case of open-channel flow and 1 for the case of confined flow. The vectors $\boldsymbol{T}$ and $\boldsymbol{R}$ for the two cases follow.

Open-channel flow

Making use of (3.1), (3.2), and (5.7*a*,*b*) results in

$$\boldsymbol{T} = \begin{pmatrix} -C_0 - \alpha^2\nu_{t0}U'_0\eta \\ \tfrac{1}{4}C_D\alpha^2 l_0^2 U_0'^2\eta \\ \tfrac{1}{4}C_D l_0^2 U_0'^2 \\ 0 \end{pmatrix}, \qquad \boldsymbol{R} = \begin{pmatrix} -\alpha^2\nu_{t0}U'_0 \\ \tfrac{1}{4}C_D\alpha^2 l_0^2 U_0'^2 \\ 0 \\ 0 \end{pmatrix}.$$

Confined flow

Since $d = -1$ and using (3.1), (3.2), and (4.4*a*,*b*) we obtain

$$\boldsymbol{R} - \boldsymbol{T} = \begin{pmatrix} C_0 + C_0[u'/U_0']_{\eta_0} - \alpha^2 \nu_{t0} U_0'(1-\eta) \\ \frac{1}{4} C_D \alpha^2 l_0^2 U_0'^2 (1-\eta) \\ -\frac{1}{4} C_D l_0^2 U_0'^2 \\ 0 \end{pmatrix}.$$

REFERENCES

BRADSHAW, P. 1987 Turbulent secondary flows. *Ann. Rev. Fluid Mech.* **19**, 53–74.

BRUNDETT, E. & BAINES, W. D. 1964 The production and diffusion of vorticity in duct flow. *J. Fluid Mech.* **19**, 375–394.

CULBERSTON, J. K. 1967 Evidence of secondary circulation in an alluvial channel. *Geological Survey Research*, US Geological Survey, Prof. Paper 575–D, pp. D214–D216.

DEMUREN, A. O. & RODI, W. 1984 Calculation of turbulence-driven secondary motion in non-circular ducts. *J. Fluid Mech.* **140**, 189–222.

DE VRIEND, H. J. 1977 A mathematical model of steady flow in curved shallow channels. *J. Hydraul. Res.* **15**, 37–54.

GERARD, R. 1978 Secondary flow in noncircular conduits. *J. Hydraul. Div. ASCE* **104**, 755–773.

HAYASHI, T., OHASHI, M. & KOTANI, Y. 1985 River flow turbulence and longitudinal vortices. In *Recent Studies on Turbulent Phenomena* (ed. T. Tatsumi, H. Maruo & H. Takami), pp. 243–259. Tokyo Institute of Technology.

HINZE, J. O. 1973 Experimental investigation of secondary currents in the turbulent flow through a straight conduit. *Appl. Sci. Res.* **28**, 453–465.

IKEDA, S. 1981 Self-formed straight channels in sandy beds. *J. Hydraul. Div. ASCE* **107**, 389–406.

IKEDA, S. 1982 Lateral bedload transport on side slopes. *J. Hydraul. Engng ASCE* **108**, 1369–1373.

JACKSON, R. G. 1976 Sedimentological and fluid dynamic implications of the turbulent bursting phenomenon in geophysical flows. *J. Fluid Mech.* **77**, 531–560.

KINOSHITA, R. 1967 An analysis of the movement of flood waters by aerial photography, concerning characteristics of turbulence and surface flow. *Photographic Surveying* **6**, 1–17.

LAUNDER, B. E. & YING, W. M. 1972 Secondary flows in ducts of square cross-section. *J. Fluid Mech.* **54**, 289–295.

MCLEAN, S. R. 1981 The role of non-uniform roughness in the formation of sand ribbons. *Mar. Geol.* **42**, 49–74.

MÜLLER, A. & STUDERUS, X. 1979 Secondary flow in an open channel. *Proc. 18th IAHR Congress, Cagliari, Italy*, pp. B19–B24.

NAOT, D. & RODI, W. 1982 Calculation of secondary currents in channel flow. *J. Hydraul. Div. ASCE* **108**, 948–968.

NEZU, I. & NAKAGAWA, H. 1984 Cellular secondary currents in a straight conduit. *J. Hydraul. Engng ASCE* **110**, 173–193.

NEZU, I. & NAKAGAWA, H. 1989 Self-forming mechanism of longitudinal sand ridges and troughs in fluvial open-channel flows. *Proc. 23rd IAHR Congress, Ottawa, Canada*, pp. B65–B72.

NEZU, I., NAKAGAWA, H. & TOMINAGA, A. 1985 Secondary currents in a straight channel flow and the relation to its aspect ratio. In *Turbulent Shear Flows IV*, pp. 246–260. Springer.

PARKER, G. 1984 Discussion of: Lateral bedload transport on side slopes, by S. Ikeda. *J. Hydraul. Engng ASCE* **110**, 197–203.

SCHLICHTING, H. 1979 *Boundary Layer Theory*. McGraw-Hill.

SPEZIALE, C. G. 1982 On turbulent secondary flows in pipes of noncircular cross-section. *Intl J. Engng Sci.* **20**, 863–872.

SPEZIALE, C. G. 1987 On nonlinear K–l and K–ϵ models of turbulence. *J. Fluid Mech.* **178**, 459–475.

TOMINAGA, A. & NEZU, I. 1991 The effects of secondary currents on sediment transport in open-channel flows. *Proc. Intl Symp. on The Transport of Suspended Sediment and its Mathematical Modelling, Florence, Italy*, pp. 253–264.

TRAVIS, J. R., BUHR, H. O. & SESONSKE A. 1971 A model for velocity and eddy diffusivity distributions in fully turbulent pipe flow. *Can. J. Chem. Engng* **49**, 14–18.

TSUJIMOTO, T. 1989 Longitudinal stripes of sorting due to cellular secondary currents. *J. Hydrosci. Hydraul. Engng* **7**, 23–34.

VANONI, V. A. 1946 Transportation of suspended sediment by water. *Trans. ASCE* **111**, 67–133.